JOURNAL OF PETROLEUM GEOMECHANICS
(JPG)

Original article

Geomechanical modelling and cap-rock integrity of one of the southwest Iranian giant carbonate oil field

Narges Saadatnia[1], Yousef Sharghi*[2], Jamshid Moghadasi[3], Mohsen Ezati[4]

1-PhD student; Faculty of Mining Eng., Sahand University of Technology
2- Associate Professor; Faculty of Mining Eng., Sahand University of Technology
3- Associate Professor; Ahwaz Faculty of Petroleum, Petroleum University of Technology (PUT)
4- Petroleum Engineering Department; SeaLand Engineering and Well Services (SLD)

Received: 2 August 2022; Accepted: 14 September 2022

DOI: 10.22107/jpg.2022.354445.1176

Keywords

**Pore pressure,
Rock mechanical model,
4-D Geomechanical modeling,
Cap-rock integrity,
One-way coupling**

Abstract

Geomechanical modeling and simulation are introduced to accurately determine the combined effects of hydrocarbon production-injection scenarios and changes in rock properties due to geomechanical effects. Pore pressure and stress states vary during production and injection steps. These variations considerably affect reservoir and cap-rock integrity, faults reactivation, formation compaction and uplifting, and wellbore stability. Therefore, accurate pore pressure estimation is essential to maintain optimal conditions during injection and production operations. A series of data, including rock mechanical test data, well logs data, formation dynamic tester data, image logs data, leak-off tests (LOTs), drilling events, and regional geological studies were used in this work. In this study, a coupled geomechanical-fluid flow model was constructed to evaluate the cap-rock integrity during the injection-production scenario. The steps of the investigation are data audit, 1-D mechanical modeling (MEMs), 3D rock mechanical properties modeling, and 4D geomechanical simulation using a one-way coupling method. The results showed that throughout the production and injection scenario, the cap-rock was stable. Since there is a long distance between Mohr's circle and the envelope, the cap-rock will not fail. Due to the low permeability of the cap-rock, there is no connection between its pore spaces, which leads to ignoring the variation in stress state due to variations in reservoir pressure.

1. Introduction

Geomechanics has become one of the most popular sciences in the research related to drilling, development, and exploitation of hydrocarbon fields throughout the world in recent decades. There are numerous advantages to improving geomechanics knowledge, such as a better specification of reservoir deformation and its impact on the rock permeability (compaction and dilation), surface subsidence, fault reactivation, and hydraulic fracture propagation throughout water flooding, or different improved oil recovery techniques. It performs a vital role in making decisions at all steps of production and enhanced oil recovery (injection process). The reservoir pore pressure is altered during the production and injection process; consequently, the stress states are changed in the various steps of the reservoir's life [1-4]. These alternations of the reservoir pressure and stress can destroy the integrity of the reservoir and cap-rock [5, 6].

Gas injection improves the reservoir pore pressure and reduces the stability of faults close to injection wells' location [7]. Therefore, the potential risks related to pre-existing faults reactivation soar due to increasing the reservoir pore pressure. Also, the fault reactivation might increase the permeability of cap-rock, which causes fluid leakages from the reservoir to the atmosphere or shallow aquifers [8, 9]. Numerous studies on reservoir geomechanical modeling show that gas injection causes significant

* Sahand University of Technology, Sahand New Town, Tabriz, Iran. Postal Code: 5331817634, Email: sharghi@sut.ac.ir

geomechanical changes in the reservoir [7, 10, 11]. Hence, constructing accurate geomechanical numerical modeling is important to determine the consequences of the production and injection processes during the reservoir lifetime. The geomechanical model is built to analyze the impact of the stress and strain on the rock compaction, structure displacement, rock deformation, and the way the rock properties (permeability and porosity) respond to reservoir pore pressure alternations due to production and injection steps, and to determine the final recovery of the reservoir under this condition. Because of the intricacy of the issues and coupled interactions between injection, production, and stress change, a comprehensive evaluation needs numerical modeling including the coupling of geomechanics with porous media fluid flow, injection, and fault behavior.

The first 4D geomechanics simulation investigation was done by Heffer et al. in 1994, to improve waterflood sweep efficiency. They coupled the geomechanical, thermal and fluid flow modeling [12]. Also, numerous pioneering studies on the 4D geomechanical simulation were carried out to assess the reservoir deformation and casing damage throughout both injection and production steps [13 and 14]. The approach for predicting microseismicity by coupled simulation was provided by Settari et al in 2002, which paved the door for microseismic controlling to establish the coupled geomechanics/reservoir-simulation outcomes [14]. The industry has progressively identified the significance of 4D geomechanics over the time, and 4D geomechanical simulations have been extensively carried out on deep-water turbidities [15], assessment of fault reactivation, well integrity in methane hydrate product [16, 17] and fractured-carbonate reservoirs [18]. Yang et al provide a 4D coupled geomechanics/reservoir simulation of a high-pressure/high-temperature naturally fractured reservoir to determine the impact of stress alternations during a long-term production [19]. A two-way coupled 4D geomechanical simulation was carried out by Ahmed et al. for a carbonate gas reservoir, to investigate the comparison between two-way coupled geomechanical simulation and conventional reservoir simulation results [20].

The pore pressure of the studied field has been greatly reduced during decades of production, so that its pore pressure is currently lower than the hydrostatic pressure. Therefore, it is inevitable to carry out pressure-maintenance activities to keep and increase production from the reservoir. By increasing the reservoir pressure during injection projects, the cap-rock may be damaged and its integrity may be lost, and oil may leak from the reservoir. In order to prevent these catastrophes, we must have a proper plan for injection into the reservoir [7]. Hence, the main aim of the current case study is to determine the cap-rock integrity during the injection-production plans.

In the present research, a sector of the studied oil field is evaluated by using a coupled hydro-geomechanical model evaluation. The hydro-mechanical model generally contains more computational steps than the only simulation of the flow equations. Such coupled model was generated by a significant number of operation techniques [21, 22]. The mentioned methods cause it plausible to simulate separate solvers for the flow and mechanical part of the problem, considering the re-use of existing as remarkably advanced simulation tools. This study is provided not only simulation analysis but also experimental results, leading to a calibrated model for having knowledge of reservoir-caprock behavior during injection and production scenarios. The scope of this case study can be divided into three main steps: 1) The first includes analysis and quality control with information from various sources to obtain necessary data and parameters to characterize the reservoir-cap rock properties, construct a 1D rock mechanical model, and create a 3D geomechanical model. 2) The second step includes the one-way coupling between a 3D geomechanical model and a dynamic flow simulation model, and 3) the third one involves obtaining the stability threshold of caprock and reservoir rock according to the Mohr-Coulomb failure criterion. The novelty of this work lies in the best utilization and matching between the gathered field data to build the 1D and 3D MEMs and to use both models to diagnose and predict future problems to be considered in any field development plans. In addition to previous stuieds, we tried to to integrate all general approaches with the geomechanical study as a new method to optimize reservoir management and evaluate capr rock integrity during production and injection scenario using VISAGE platform, which is also considred as the novelty of our work. Also, this case study can be applied on underground gas storage, CO_2 sequestration, and geothermal projects in the studied area.

2. Geological Setting

The Zagros Orogen is the result of three main consecutive geotectonic events including subduction of the Neo-Tethyan oceanic plate beneath the Iranian lithospheric plates during Early to Late Cretaceous times, emplacement or obduction of some Neo- Tethyan oceanic slivers (ophiolites) over the Afro-Arabian passive continental margin in Late Cretaceous (Turonian to Campanian) times, and collision of the Iranian plates in Late Cretaceous and later times with the Afro-Arabian continental lithosphere [23]. The orogen is surrounded by the East Anatolian left-lateral strike-slip fault (EAF) and the Oman Line (OL) in the northwest and the southeast, respectively [24]. The orogen is structurally composed of three parallel belts (the Zagros fold-thrust zone, the imbricate zone, and the Urumieh-Dokhtar magmatic assemblage) from southwest to northeast, respectively. It has an irregular geometry such as the Fars salient, the Dezful recess, the Lorestan salient, and the Karkuk recess from southeast to northwest, respectively (**Error! Reference source not found.**).

The oil field under investigation is one of Iran's major oil fields with more than 45 billion barrels of oil-in-place, located in Dezful-Embayment in southwestern Iran. The study oil field has a complicated structure in the region. It should be pointed out that each part of this field has different production conditions because of intense faulting and erosion and/or deficiency in sedimentation for the cretaceous sequence on the eastern flank. The study oil field is one of the most active oilfields in two Oligocene-Miocene and middle Cretaceous carbonate (Cenomanian–Turonian) horizons that show the Asmari and Sarvak formations, respectively [25]. 85% of total Iran's hydrocarbon reserves are located in the Asmari formation. The combination of rich source rocks (Kazhdumi and Pabdeh Formations), permeable and porous reservoirs (Asmari and Sarvak–Illam), and a proper cap-rock (Gachsaran and Gurpi Formation) creates ideal conditions to form a rich petroleum province in Zagros and particularly in Dezful Embayment.

Asmari Formation is composed of cream to gray limestone, dolomitic limestone, and dolomite with a thickness of 314 m in the type section [26]. Gachsaran Formation with an age of Miocene comprises seven members named by numbers 1 to 7 from base to top. Member 1 (the lowermost member) is considered a cap-rock that overlies the Asmari reservoir [27]. It mainly contains lithologies of anhydrite, bituminous shale, gray marl, and limestone [27 and 28]. The location of the investigated oil field and its simple geological column are shown in Fig. 1. Based on the 2D seismic data interpretation by NISOC (National Iranian South Oil Company),, two faults have been extracted in the study sector of the field. Each fault was marked with a number as displayed in Fig. 2.

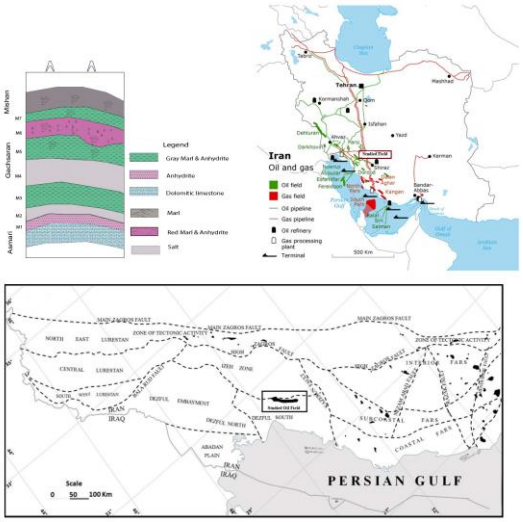

Fig. 1 Location and stratigraphic column of study oil fled in Zagros fold-thrust belt

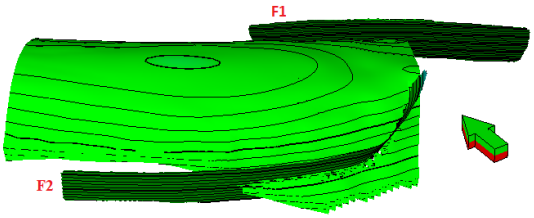

Fig. 2 Detected faults in the studied sector

3. 1-D Geomechanical Model Construction

The geomechanical model is a numeric demonstration of the rock's mechanical features and stresses situation adjacent to the well. The basis for evaluating the cap-rock integrity is a geomechanical well model construction and the investigation of these models. A rock mechanical model contains deep profiles such as elastic parameters, rock strength, pore pressure, and the magnitude and direction of in situ stresses [29]. The prime stage of the study includes quality

control of data and creating 1-D mechanical earth models (1-D-MEM). The parameters such as rock strength and deformation (Young's modulus, Poisson's ratio, shear and bulk moduli), horizontal and vertical stresses, and pore pressure are estimated in a 1-D geomechanical model [30]. This 1-D model use data observation of both directions and magnitudes of stress (e.g., breakout directions, induced fractures, and LOT (leak-off-tests) in combination with drilling experience and the utilized mud weights) to create the stress models along the well trajectory and are then applied as calibration points for the 3-D geomechanical model. The overall workflow of 1-D geomechanical modeling is shown in Fig. 3.

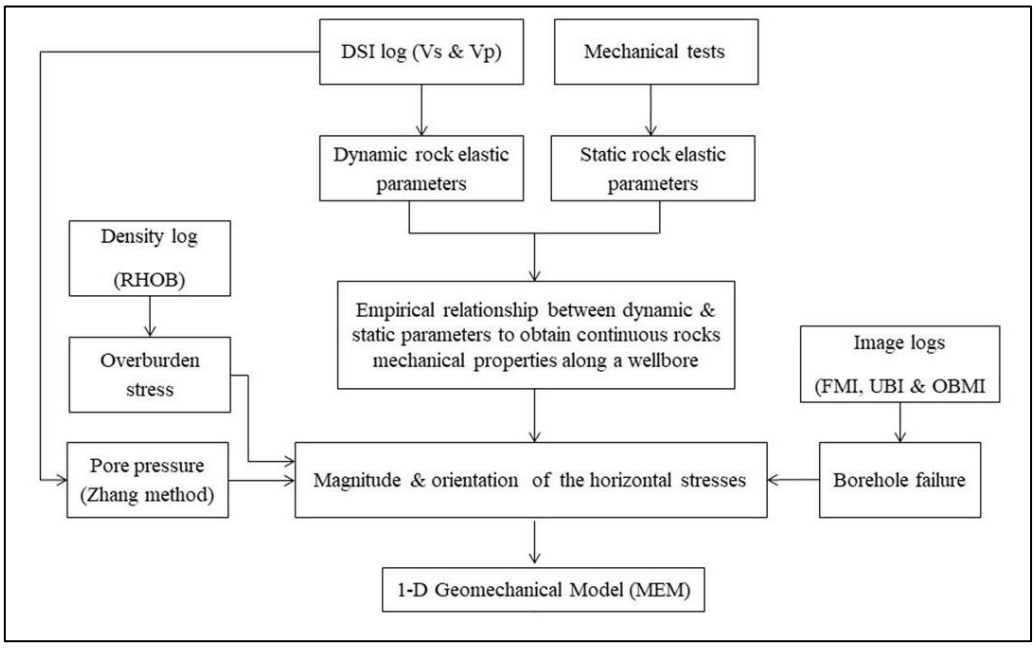

Fig. 3 The general workflow which used for 1-D geomechanical models

The dynamic rock properties including Poisson's ratio (ν_d) and Young's modulus (E_d) can be determined using compressional and shear waves velocities (V_P & V_S) and density of rock (ρ) as following formula [29]:

$$E_d=\rho V_S^2 \frac{3V_P^2-4V_S^2}{V_P^2-V_S^2} \quad (1)$$

$$\nu_d=\frac{V_P^2-2V_S^2}{2(V_P^2-V_S^2)} \quad (2)$$

The elastic parameters acquired from dynamic and static techniques are regularly different. Typically, in the dynamic condition, the obtained elastic parameters have high values, so dynamic values should be converted to static values using rock mechanical tests [30]. Static parameters are more realistic than dynamic parameters and they are widely used in geomechanical modeling [31]. However, static parameter measurement is more arduous than dynamic parameters. Therefore, providing the empirical correlations between dynamic and static parameters is essential for the reliable and continuous prediction of rocks' mechanical properties along a wellbore. There are numerous empirical correlations between dynamic and static parameters such as Lacy 1996, Ameen et al., 2009 and Asef and Farrokhrouz 2010, which were obtained based on local information, and are not able to cover a wide range of lithology [31-33]. In this regard, providing local relations for specific lithology is always preferable to general correlations. Hence, In this study, static Young's modulus (E_s) and uniaxial compression strength (UCS) were achieved from the uniaxial tests on 11 plug samples collected from the Asmari reservoir and cap-rock. The ASTM D3148–93 standard was followed for the uniaxial tests. For the uniaxial tests, the plugs were placed in a loading frame. Axial load was increased on the core sample at a

constant and continuous rate, while axial and lateral deformations were monitored as a function of load. The results of uniaxial tests are shown in Table 1.

In addition, dynamic Young's modulus was measured using V_P, V_S, acquired from the dipole shear sonic log (DSI) at the same depths that core samples were taken. The best correlation between E_s and E_d, as well as UCS and E_d, are obtained as follows (**Error! Reference source not found.**):

$$E_s = 0.057677 E_d^{1.5751} \quad (3)$$

$$UCS = 0.0925 E_d^{1.6802} \quad (4)$$

Table 1. The results of uniaxial tests on the 11 plug samples

Sample ID	Diameter (mm)	Length (mm)	Ed(50) (GPa)	Es (GPa)	UCS (MPa)	Lithology
S-1	38.23	79.60	47.0856	34.89	78.98	Limy Anhydrite
S-2	38.30	72.25	79.69916	59.13	133.5	Anhydrite
S-3	38.25	79.27	84.10949	57.79	169.9	Anhydrite
S-4	38.31	80.10	84.10949	58.64	167.5	Anhydrite
S-5	38.33	80.26	83.77245	61.9	178.5	Anhydrite
S-6	38.25	76.83	82.45716	70.48	176.3	Dolomite
S-7	38.25	78.52	82.51546	75.23	177	Dolomite
S-8	38.32	79.26	59.62445	34.87	89	Limestone
S-9	38.31	72.62	76.03781	58.59	154.9	Nodular dolomite
S-10	38.26	79.02	62.87649	27.88	68.47	Sandy Limestone
S-11	38.25	77.52	62.87649	27.35	76.45	Sandy Limestone

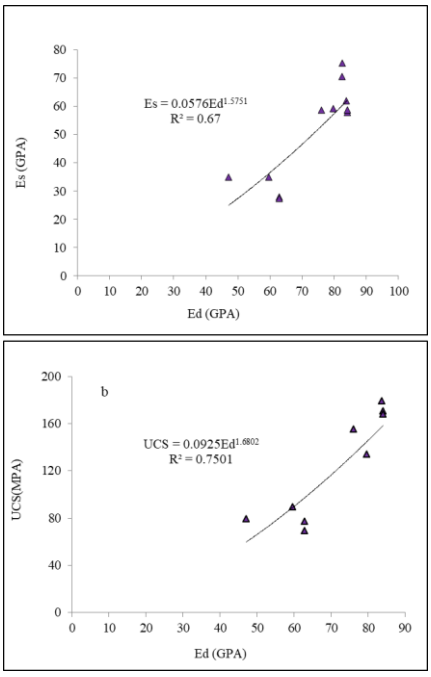

Fig. 4 The correlations which extracted between a) E_s and E_d; b) UCS and E_d

To check the validity of the obtained relationship, the derived equation for one of the nearby fields, established by Seyed Sajjadi and Aqiqi (2014) (Eq.5), was utilized [34]. Also, since the study reservoir formation in the studied field contains carbonate lithology, Ameen's correlation (Eq.6) and Asef 's correlation (Eq.7), developed for carbonate rocks, were used as the validation for equations 3 and 4, respectively [32, 33]. **Error! Reference source not found.** illustrate Young's modulus calculated by Equations 3, 5, and 6. As it can be seen, the static Young's modulus estimated by Equations 3, 5, and 6 (E_{s1}, E_{s2} and E_{s3}) show a good overlap. Beside the good match obtain between Equations 3 (UCS1) and Equations 7 (UCS2).

$$E_s = 0.731 E_d + 2.337 \quad (5)$$

$$E_s = 0.541 E_d + 12.852 \quad (6)$$

$$UCS = 2.65\left(\frac{E_s^{0.8}}{PHIE^{0.2}}\right) \quad (7)$$

Also, cohesion (c) and friction angle (φ) are other

mechanical properties that describe the intrinsic properties of rocks. These two parameters may be measured by performing a laboratory triaxial test on the core plugs. Moreover, there are empirical equations to friction angle and cohesion prediction when there is no access to the triaxial test [35 , 36]:

$$\varphi = 26.5 - 37.4(1 - \mathrm{NPHI} - V_{sh}) + 62.1(1 - \mathrm{NPHI} - V_{sh})^2 \quad (8)$$

$$c = \frac{\mathrm{UCS}}{2\tan\left(45 + \frac{\varphi}{2}\right)} \quad (9)$$

where φ is friction angle (degree), c is cohesion (MPa), NPHI is neutron porosity, UCS is uniaxial compressive strength (MPa), V_{sh} is shale volume obtained from GR log.

The information about initial pore pressure is crucial to calculate in-situ stress magnitudes, wellbore stability, and discontinuity reactivation analysis throughout depletion and injection. Pore pressure is a vital parameter which could be measured using in-situ tools such as MDT (Modular Formation Dynamics Tester), RFT (Repeat Formation Tester), and DST (Drill Stem Test) data. There are several empirical approaches in the literature for in-situ pore pressure estimation. In the oil industry, different methods such as Eaton, Holbrook, and Bowers are used to calculate pore pressure [30]. Amongst various approaches, Eaton's method is a prevalent equation to compute the pore pressure, which is specified as follows [37]:

$$P_{Pg} = S_V - (S_V - P_{Hyd})\left(\frac{DT_n}{DT}\right)^3 \quad (10)$$

where P_{Pg} and S_V are pore pressure and vertical stress gradient, respectively. P_{PHyd} is hydrostatic pore pressure gradient, DT_n is the sonic transit time in shales with a normal pore pressure and DT is sonic transit time. The NCT is the normal compaction trend of the sediments estimated by fitting a curve to the sonic transit time log. Equation 6 shows Eaton's equation for estimation of pore pressure modified by Zhang (2011) with replacing DT_n with following equation [38].

$$DT_n = DT_m + (DT_{ml} - DT_m)e^{-cZ} \quad (11)$$

with zero porosity, DT_{ml} is P wave slowness in mud line, c represents an experimental constant, and Z shows the depth. Parameter c represents an empirical constant, and Z is the depth. According to the study of Azadpour et al. (2015) on some carbonate reservoirs, the modified Eaton method was proposed as an appropriate approach to predicting pore pressure in these reservoirs [39]. Therefore, prediction of pore pressure in the studied reservoir (Asmari carbonate formation) was calculated by this method. In this paper, the initial pore pressure was estimated based on the modified Eaton method. Also, MDT (modular formation dynamics tester) tool was run in the wells, which measured downhole formation pressure against various target formations, as chosen by the operator. These MDT points are the direct in situ pore pressure measurements and yield the most reliable PP calibration. As it can be seen in Fig. 5, there is a good correlation between MDT points (black points in track 10 Fig. 5). and predicted pore pressure curve.

The magnitude of overburden stress (S_V) is calculated using the following equation [30].

$$S_V = \int_0^z \rho(z) g \, dz \quad (12)$$

where ρ(z) expresses the average formation bulk density as a function of depth, z represents depth and g is the acceleration due to gravity (Earth's gravity acceleration).

Evaluating the magnitudes of the maximum and minimum horizontal stresses (S_{Hmax} and S_{hmin}) is a major challenge in geomechanical modeling. Several practices are proposed to estimate the minimum horizontal stress such as creating hydraulic failure in the well wall, extended leak-off test (XLOT), and leak-off test (LOT). LOTs are conducted after the casing has been cemented in place and the casing shoe is drilled out a short distance (~5 m) [30]. Usually, in the LOT by injecting drilling mud as an injection fluid into a well, crack opening pressure is considered as the minimum in situ stress. The obtained values from this method are discontinuous. Hence, the poroelastic equations are used to estimate the Hence, the poroelastic equations are used to estimate the continuous magnitudes of the horizontal stresses (S_{Hmax} and S_{hmin}) along the well [29]:

$$S_{hmin} = \frac{\nu}{(1-\nu)}(S_V - \alpha PP) + \alpha PP + \frac{E_S}{(1-\nu^2)}\varepsilon_x + \frac{\nu \times E_S}{(1-\nu^2)}\varepsilon_y \quad (13)$$

$$S_{Hmax} = \frac{\nu}{(1-\nu)}(S_V - \alpha PP) + \alpha PP + \frac{E_S}{(1-\nu^2)}\varepsilon_y + \frac{\nu \times E_S}{(1-\nu^2)}\varepsilon_x \quad (14)$$

where, ν is Poisson's ratio, S_V is overburden pressure, α is Biot's effective stress coefficient, PP is pore pressure and E_S is static Young's modulus. The tectonic strain on x (ε_x) and y (ε_y) axes are determined by the following equations [40]:

$$\varepsilon_x = \frac{S_V \times \nu}{E_S}\left(\frac{1}{1-\nu} - 1\right) \quad (15)$$

$$\varepsilon_y = \frac{S_V \times \nu}{E_S}\left(1 - \frac{\nu^2}{1-\nu}\right) \quad (16)$$

Appropriate values for the two horizontal strains and, hence, the two horizontal stress magnitudes, can be found by fitting these values to observational data on in situ stress magnitudes, e.g., from LOT [41].

Moreover, a limited number of available cores in most drilled wells limits the possibility of the experimental evaluation of the material parameters. This, therefore, has particularly made it difficult to evaluate a continuous profile of Biot's effective stress coefficient in the wells. So, it is interesting to obtain alternative methods to evaluate the profile of the Biot's effective stress coefficient using the available information in the wells (e.g., wave velocity, porosity, mineralogical composition, etc.). Hence in the studied area, the Biot coefficient was determined from empirical relationship based on effective porosity (PHIE) [42]:

$$\alpha = 1 - (1 - PHIE)^{3/(1-PHIE)} \quad (17)$$

In this study, the magnitude of vertical in-situ stress was calculated using Eq. (7). Furthermore, poroelastic equations were used for continuous estimation of the horizontal stresses (S_{Hmax} and S_{hmin}) magnitudes along the well profile (track 10 in **Error! Reference source not found.**). Also, the calculated minimum horizontal stress from poroelastic horizontal strain model was validated by direct measurements of the LOT data (red points in track 10 Fig. 5).

The next step is finding the direction of horizontal stresses. Image logs are useful tools to detect the borehole breakouts and drilling-induced tensile fractures which are caused by wellbore hoop stress and radial stress, respectively [30]. Drilling-induced fractures and Borehole breakouts are both significant indexes to estimate horizontal stress direction. In vertical wells, the breakouts form at the azimuth of the minimum horizontal stress (S_{hmin}), and drilling-induced tensile fractures take place in the wall of the borehole at the azimuth of the maximum horizontal stress (S_{Hmax}), when the circumferential stress acting around the well is locally in tension. According to the available image logs including OBMI (oil-base micro-imager), UBI (ultrasonic borehole imager), and FMI (formation micro-imager), the azimuth of principal horizontal stresses was determined in the study area. In this paper, the direction of horizontal stresses was computed by using a large number of breakout observations in the image logs. Borehole breakouts are represented over image logs using box shapes, the central axis of which shows the direction of the minimum horizontal stress (Fig. 6a). Based on the breakouts' orientation, the S_{hmin} and S_{Hmax} directions of the studied wells are N55.5°W and N34.5°E, respectively (Fig. 6b). Finally, the estimated parameters of rock elastic properties, pore pressure, and in situ stress were plotted using proper well logs combinations and are presented as a 1-D geomechanical model for each well. Based on Anderson's fault theory, the stress regimes are as followings [30]:

- Normal stress regime ($S_v > S_{Hmax} > S_{hmin}$)
- Strike-slip stress regime($S_{Hmax} > S_v > S_{hmin}$)
- Reverse stress regime ($S_{Hmax} > S_{hmin} > S_v$)

As it can be seen in **Error! Reference source not found.**, S_v is the maximum principal stress (σ_1), S_{Hmax} is the intermediate one (σ_2), and S_{hmin} is the minimum principal stress (σ_3). According to Anderson's faulting theory the tectonic stress regime in the Asmari reservoir is a normal stress regime ($S_V > S_{Hmax} > S_{hmin}$) while in-situ stresses values are very close to isotropic condition in the caprock. Also, based on the image logs interpretation, S_{Hmax} directional is approximately

perpendicular to the fracture's strike. In the way that S_{Hmax} directional is NE-SW and the strike of all open fractures is NW-SE.

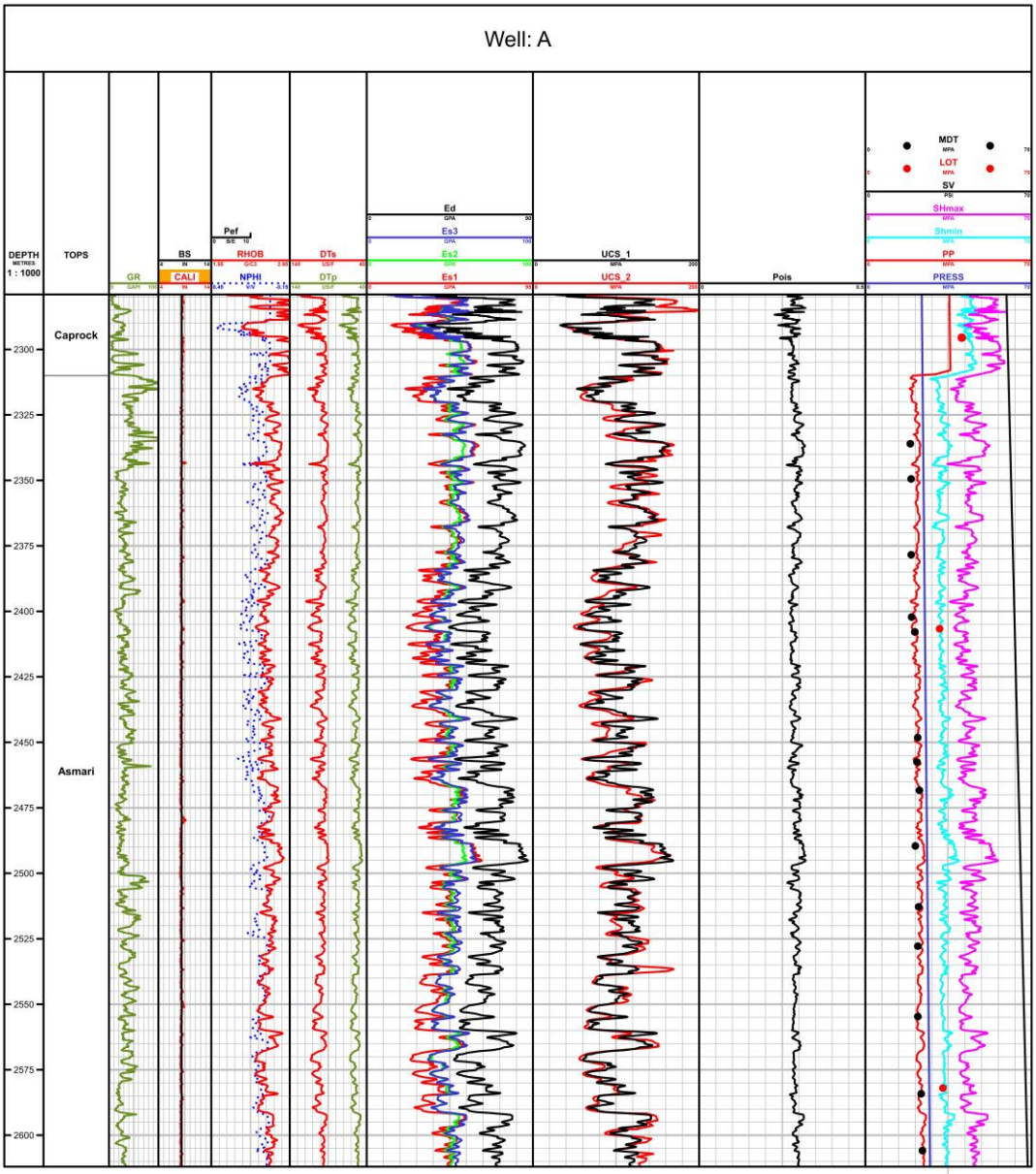

Fig. 5 The 1-D geomechanical model which conducted for one of the study. (Track 3 to Track 6) Petrophysical raw data (GR, Bit size and caliper, bulk density and neutron porosity, compressional and shear slowness). (Track 7 to 9) Calculated rock mechanical properties (Static and dynamic Young modulus, Poisson's ratio, UCS: Unconfined Compressive Strength). (Track 10) In situ stress calculation and pore pressure prediction

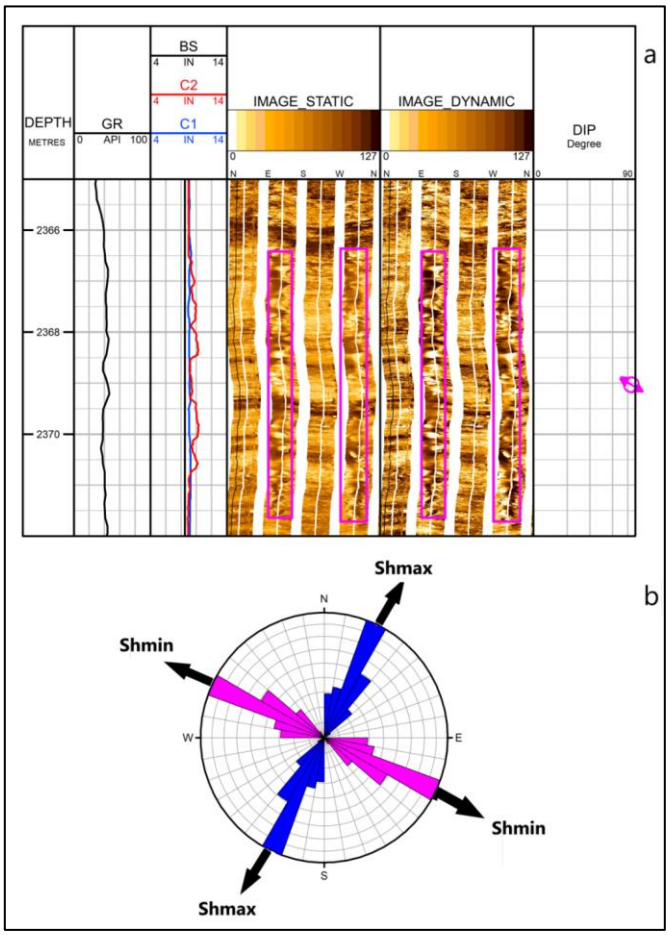

Fig. 6 a) A pair of breakouts on image logs, b) S_{hmin} and S_{Hmax} directions from borehole breakouts interpretation

4. 3-D Geomechanical Modeling and One-Way Coupling

In the second phase, the 3-D static and dynamic models were built by the Petrel software. 3-D geomechanical models were constructed using the VISAGE platform. The VISAGE finite element platform was utilized to perform the numerical stress and displacement determination. Afterward, the 3-D geomechanical model was coupled to a dynamic (simulation) model using the one-way method. The construction of a 3-D geomechanical model is performed along with a one-dimensional geomechanical model to obtain a comprehensive 4-D geomechanical model. All these workflows are important to assess stress state, cap-rock integrity. A series of key data including rock mechanic tests, well logs data, 1-D mechanical earth model results, geological (static) model, dynamic (simulation) model, and regional geological study were used to create a 4-D geomechanical model. The workflow steps for creating a 4-D geomechanical model are geomechanical gridding (overburden, under-burden, and side-burden), making the geomechanical materials (material modeling), populating properties, discontinuity modeling, defining boundary conditions, and defining reservoir simulation case. In the prime step, to simulate the accurate values of the vertical and horizontal stresses, the 3-D geological (static) model is converted to an embedded model by adding the overburden, sides-burden, and under-burden to it. Embedding is an essential procedure to make sure that boundary effects do not have an impact on the stress state in the reservoir area. Overburden-layers consist of the grids that start from the top of the reservoir to the surface, and the under-burden contains the grids from the bottom of the reservoir to any desired depth. In this investigation, the overburden grids include cap-

rock and overburden layers (Gachsaran and Mishan formations). Also, thickness of the under-burden layer was considered more than the reservoir grids to prevent buckling during the loading. To reduce the run-time, the sizes of side-burden grids, which are located around the reservoir, were taken larger than the reservoir model grids. In this study, 5 grids from each side have been added to the reservoir model. The mechanical properties of side-burden were assumed same as the reservoir. Furthermore, two plates are jointed as a competent rock around the sideburdens to change the sides-burden uniformly. Fig. 7 illustrates the geomechanical grids of study area. The constructed three-dimensional geomechanical model includes a total of 275502 grid cells.

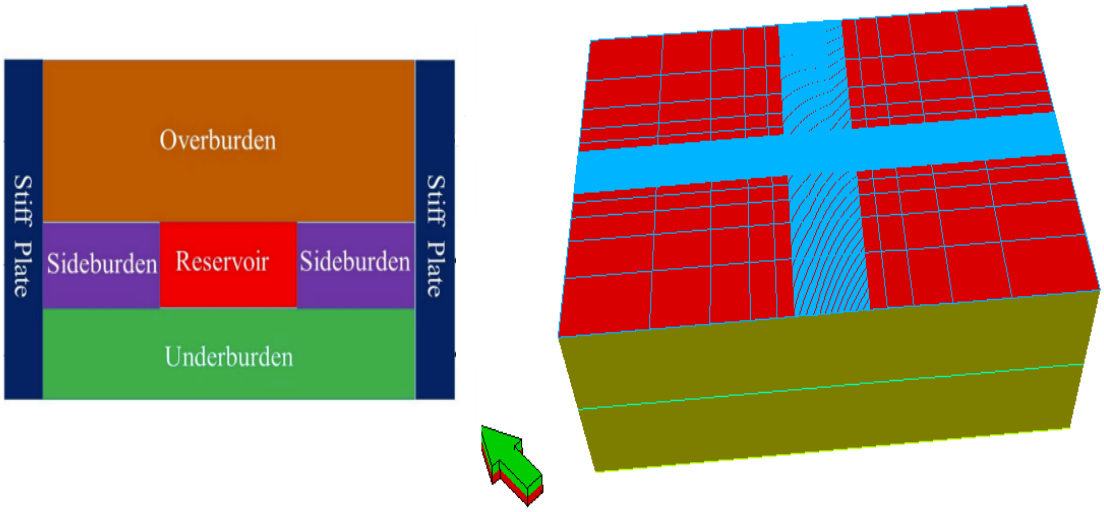

Fig. 7 The constructed geomechanical grid including overburden, underburden, side-burden and reservoir for the studied field

It is worth to mention that the 1-D geomechanical logs were upscaled through the geostatistical methods to the model well grids. Then the upscaled logs were interpolated using the 3D model by the Gaussian simulation. In the material modeling step, the material parameters from the 1-D MEM results were set to the 3D geomechanical grids. The materials can be specified as linear or nonlinear and consist of linear elastic parameters and failure criteria (Mohr-Coulomb, Tresca, Drucker-Prager, etc.). Two types of material are described as follows:

- Intact rock material for the reservoir, side-burden, overburden, and under-burden, according to the variety of elasticity models and yield criteria.
- Discontinuity materials, for modeling both fractures and faults.

The next step is populating geomechanical properties. In this study, continuous properties (static Young's modulus, UCS (unconfined compressive strength), Poisson's ratio, etc.), derived from the 1-D MEM logs, were populated in each cell of the model. For creating 4D geomechanical model, all 1-D MEM logs were up scaled and then propagated in 3D static model using applying statistic methods. All mechanical parameters and bulk density models of the reservoir formation were modeled (Fig. 8).

In discontinuity modeling, a fault mapping object illustrates how the mentioned model relates to a set of faults. All created objects comprise a set of fault attributes and a list of cells grids that interlace with the faults. It is essential to calculate the geomechanical properties of the faults (such as cohesion strength (c) and the coefficient of static friction (μ)) to evaluate faults activation, but there is no data about faults properties in this study. It is suggested that in the lack of faults data, the static friction coefficient can be considered equal to 0.6 [30 and 43]. In the next step, pressure, temperature, and saturation (PTS) condition is defined for a distinct simulation case at different time steps. In this paper, a one-way coupling model was used, and the distribution of the

reservoir pressure was obtained from the dynamic (simulation) model. The five steps time 2020, 2025, 2030, 2035 and 2040 of simulation case scenario have been conducted in the study area. The temperature has a small effect on the estimated stresses and is therefore not apply in this study. In the 'define boundary conditions' step, the stress gradients on the geomechanical grids and the initial stress are defined. The value and direction of principal stress (S_v, S_{Hmax} and S_{hmin}) were calculated in 1-D MEM. One of the key calibration methods is a good match between calculated stresses from the 3-D geomechanical model and estimated stresses from the 1-D MEM. By using 1-D geomechanical models, the boundary condition of the horizontal stresses was determined, and the horizontal stresses of the 3-D model were tuned. Finally, in the reservoir geomechanics simulation case, all data from previous steps are imported to this model.

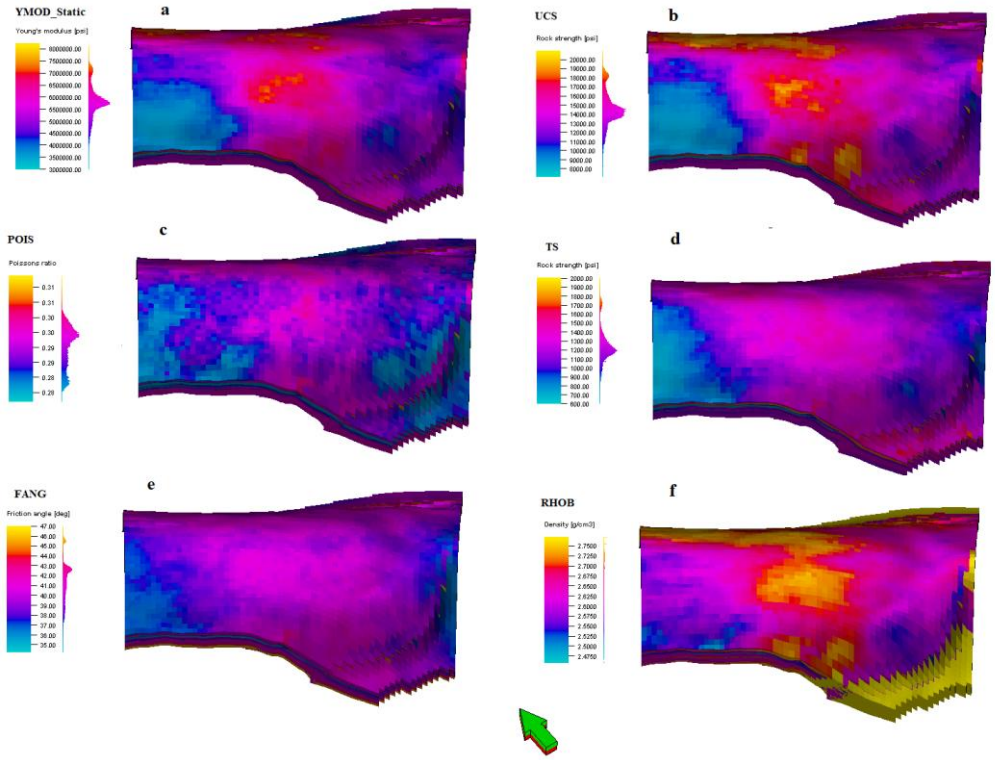

Fig. 8 The rock mechanical properties models of the studied Asmari reservoir. a) Young modules, b) UCS, c) Poisson's ratio, d) Tensile strength, e) Friction angle and f)RHOB

5. Results and Discussion

One of the most significant parts of 4-D geomechanical modeling is the coupling pattern. One-way, two-way, interactive, fully coupled and other coupling approaches vary in the method of solving the geomechanical and the fluid flow equations [44]. In the fully coupled method, geomechanical and flow simulations are run simultaneously in different pre-selected time steps. This method is a precise solution but has considerable computational complexity and long computational time [45 and 46]. In this study, the one-way coupling model was built and the pore pressure distribution was obtained from the simulation (dynamic flow) model (Fig. 9). Afterward, the fluctuations of strain via effective stress were determined as a result of pore pressure variations due to production and injection periods. After characterizing the cap-rock in the studied model (Fig. 10) the integrity of the cap-rock was evaluated using stress charting tool. In the injection and production stages, due to changes in pore pressure and effective stress reduction, the Mohr's circles moved to the left and came close to the failure envelope but did not intersect with

it. Fig. 11 shows the Mohr diagram of stress changes in the cap-rock. It is clearly shown that stress circles were on the positive side and below the failure envelope after injection and production. It means that cap-rock was in shear form with less possibility of matrix deformation and remained intact in the assumed flow rates. In this scenario, the values of cohesion and the internal friction angle are equal to 23.1 MPa and 40 degrees, respectively (Fig. 11)

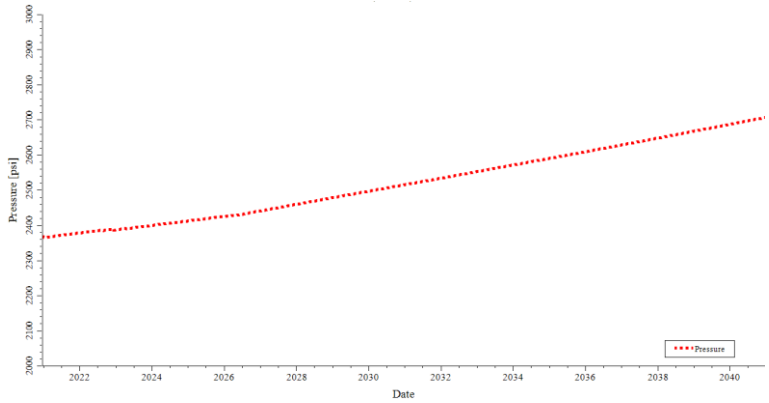

Fig. 9 The average reservoir pressure through the two production and injection periods

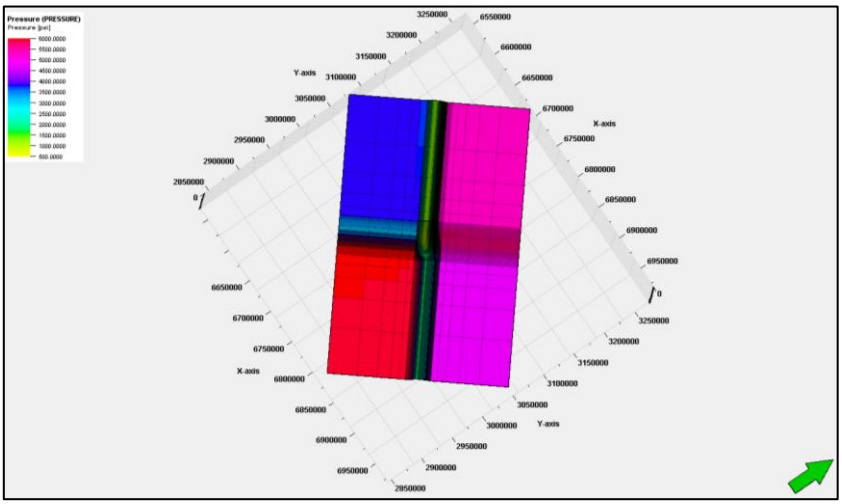

Fig. 10 Geomechanical model of cap-rock in the studied field

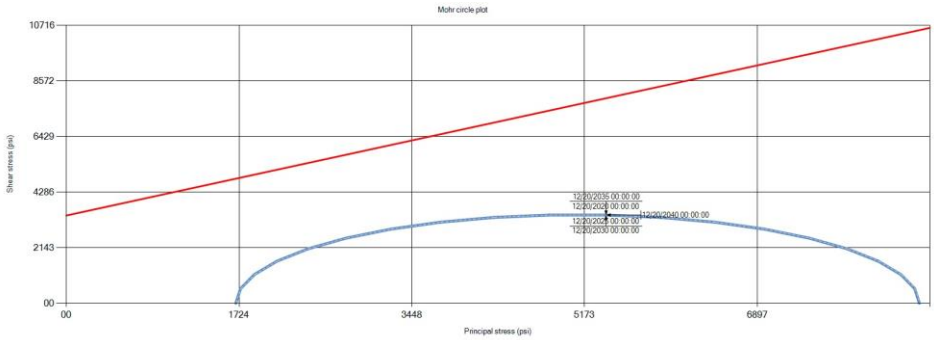

Fig. 11 The Mohr's circle distance from envelope for the cap-rock during production and injection stages

According to the amount of intercept (cohesion) and slop (internal friction angle) of the failure

envelope, it is expected that Mohr circles never meet the failure line unless the cap-rock has very low cohesion and internal friction angle values. For example, in Fig. 12, if the cohesion has a value about 1000 psi and the internal friction angle consider 10 degrees, then the cap-rock will have a shear rupture. Also, as shown in Fig. 11, the minimum effective principal stress had always a positive value. For initial effective stress of 2155 psi after 20 years of injection and production, the minimum effective principal stress was stable and had no change due to low pressure fluctuation. Therefore, the tensile rupture did not occur in cap-rock. However, if the higher injection and production rates are used, the minimum effective principal stress has the potential to be negative.

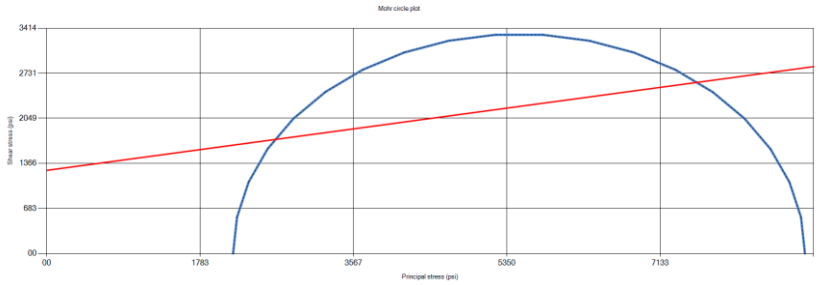

Fig. 12 Mohr circles of the cap-rock at the very low cohesion and internal friction angle values

To specify the stability of the cap-rock, the pressure of the reservoir was enhanced (Fig. 13). In each grid, the Mohr-Coulomb circle is determined based on its pressure. At the pressure equal to15474 psi, reservoir lost integrity, but the cap-rock remains stable because of the poor hydraulic continuity between the reservoir and cap-rock formations. The cap-rock acts as a sealed pressure due to poor hydraulic connection resulted from low fluid availability (porosity) and fluid mobility (permeability). Therefore, the more stiffness value of the cap-rock causes the more strength of the cap-rock at such pressure. Hence, the lack of hydraulic connection and more stability of the cap-rock were caused the cap-rock's integrity in the applied pressure range.

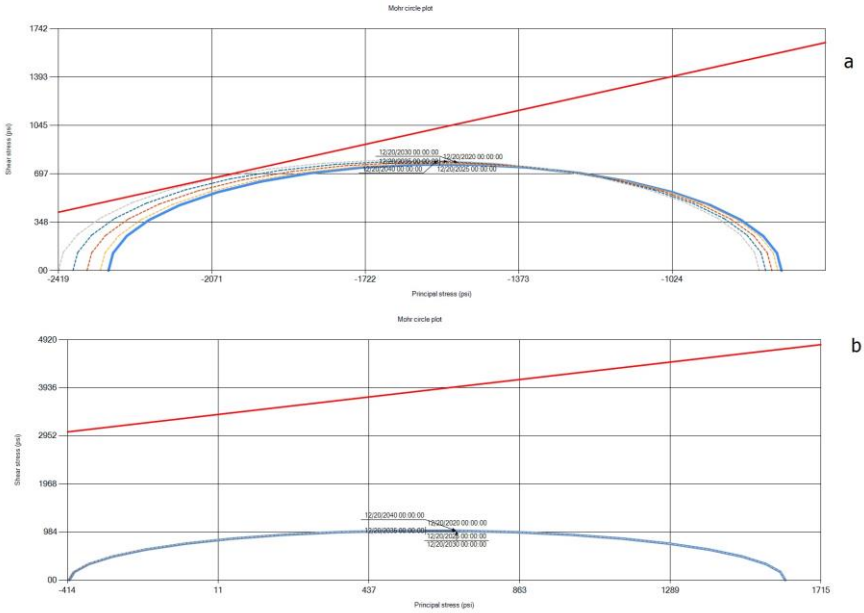

Fig. 13 The integrity of the reservoir (a) and cap-rock (b) at the critical pressure that reservoir lost its integrity

Fault reactivation is another critical aspect of geomechanical consideration to evaluate the stability rock and determine the threshold fluid pressure to reactivation of faults in formation rock (Kim et al., 2014). When the pore pressure increases, the effective normal stress will significantly decrease; consequently, prediction of critical pore pressure, which induces slip on the fault plane, is a mandatory step to safety injection scenario. Faults are modelled as discontinuities, represented by a list of grid cells which intersect with the fault. Different material properties are assigned to each cell of the faults, such as dip value, dip direction, normal stiffness, shear stiffness, cohesion, friction angle, dilation angle and tensile strength. In this study, the rock's failure criterion was determined based on the Mohr-Coulomb failure criterion, and for each cell belonging to a fault the distance to the failure envelope was calculated. Assumptions for the studied field lead to assign a static friction coefficient of 0.6 and a value of 0.001MPa for cohesion, thus considering them almost cohesionless (van Ruth et al. 2007).

Based on Mohr's circles' results in points near to main faults, there is no critical faults reactivation and none of the fault cells reach the failure envelope (Fig. 14). Moreover, Fig. 15 illustrates a non-significant change in fault elastic shear displacement during studied scenario. The examination helps to understand the critical stress nature of the faults in order to address practical field problems such as changes in field production and injection behavior. So studied simulation periods could be done safely without any faults slips in the studied field.

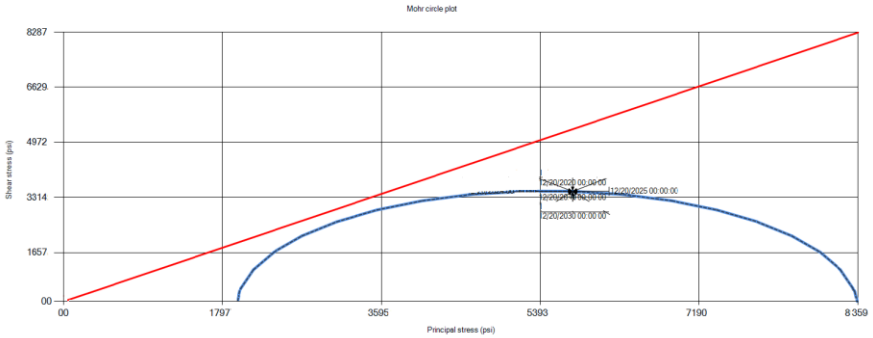

Fig. 14 Mohr–Coulomb diagram of cell within fault in the studied field

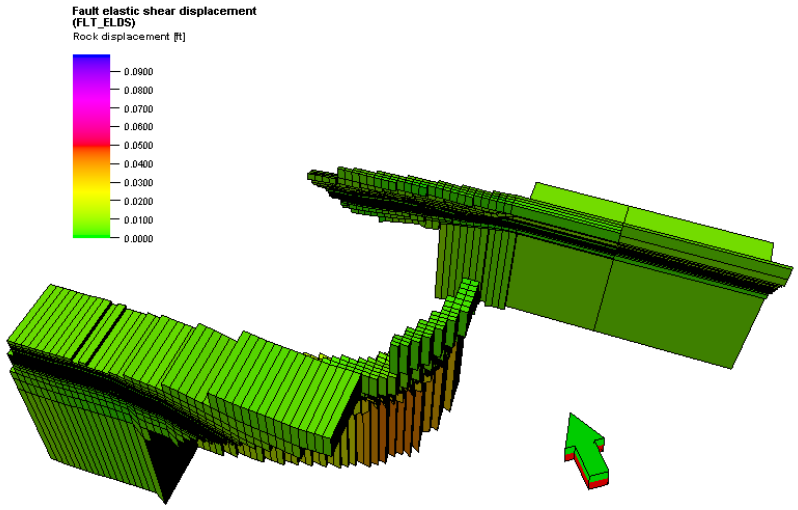

Fig. 15 Fault elastic shear displacement at simulation periods

The average initial pore pressure in the reservoir was 3471 psi. Due to production of field, pore

pressure has been dropped 1270 psi ($\Delta Pp = -1270$ psi) in this field. According to the studied case scenario, the minimum production pressure was assumed 1700 psi and the maximum injection pressure was also considered 6000psi based on related studies. Moreover, rates of field production and injection are 70000 STB/d and 549 MMSCF/d, respectively. Also, in this scenario the reservoir pressure increased from 2350 psi to 2710 psi which shows that the cap rock, reservoir and faults are stable.

6. Conclusion

To ensure the maintenance of the impermeable boundaries integrity such as cap-rock, it is essential to do investigations and geomechanical analyses throughout the production or injection from/in the reservoir. This investigation aimed to construct an efficient coupled hydro-mechanical numerical model to assess cap-rock integrity. In the hydro part, the reservoir (simulation) modeling was utilized to take the reservoir pressure distribution. In the other part, geomechanical modeling was used to obtain the stress distribution. A data set such as geological, geomechanical, and reservoir simulation result was utilized to construct the numerical 4D geomechanical simulation model. The key results obtained for the study area in this analysis are as follows:

The stress path and standard Mohr's failure envelope for cap-rock clearly show that stress circles are below the failure envelope, which indicates that the cap-rock remains intact in injection and production scenario.

For effective stress of 2155 psi after 20 years of injection and production, the minimum effective principal stress was stable and had no change due to low pressure fluctuation. Therefore, the tensile rupture did not occur in cap-rock. On the other hand, it can be concluded, over the higher injection and production rates, the instability of cap-rock gradually rises and finally the rapture occurs in cap-rock.

Throughout production and injection, the cap-rock was stable due to the low permeability and porosity of cap-rock. Because of the low permeability, there is no connection between pore spaces of the cap-rocks; therefore, it leads to ignoring the variation in stress state due to variations in reservoir pressure.

Modeling results suggest that faults failure is not a factor of risk under the calculated present-day stress conditions and the current assumptions regarding fault properties and the Mohr Coulomb failure criterion.

7. Acknowledgements

The authors wish to thank National Iranian South Oil Company (NISOC) for providing field data and permission to use it in this work.

8. Conflicts of Interest

The authors declare that they have no conflicts of interest regarding the material included in this manuscript.

9. Nomenclature

BS: Bit Size
CALI: Caliper
DSI: Dipole Shear Sonic Imager
DT_P: Slowness of compressional wave
DT_S: Slowness of shear wave
E_d: Dynamic Young's modulus
E_S: Static Young's modulus
FMI: Fullbore Formation Microimager
g: Earth's gravity acceleration
GR: Gamma ray
NPHI: Neutron Porosity
P_P: Pore pressure
RFT: Repeat Formation Tester
RHOB: Bulk Density
S_{Hmax}: Maximum horizontal stress
S_{hmin}: Minimum horizontal stress
S_V: Vertical stress
V_P: Compressional wave velocity
V_S: Shear wave velocity
ν: Poisson's ratio
ρ: Rock density
UCS: Uniaxial compressive strength
Φ: Friction angle
C: Cohesion

10. References

[1] Deflandre, J. P., Estublier, A., Baroni, A., Fornel, A., Clochard, V., & Delépine, N. (2013). Assessing field pressure and plume migration in CO2 storages: application of case-specific workflows at in Salah and Sleipner. Energy Procedia, 37, 3554-3564.

[2] Zhou, X., & Burbey, T. J. (2014). Distinguishing fluid injection induced ground deformation caused by fracture pressurization from porous medium pressurization. Journal of Petroleum Science and

Engineering, 121, 174-179.

[3] Selvadurai, A. P. S., & Kim, J. (2016). Poromechanical behaviour of a surficial geological barrier during fluid injection into an underlying poroelastic storage formation. Proceedings of the Royal Society A: Mathematical, Physical and Engineering Sciences, 472(2187), 20150418.

[4] Ezati, M., Azizzadeh, M., Riahi, M. A., Fattahpour, V., & Honarmand, J. (2020). Wellbore stability analysis using integrated geomechanical modeling: a case study from the Sarvak reservoir in one of the SW Iranian oil fields. Arabian Journal of Geosciences, 13(4), 1-19.

[5] Chan, A. W., & Zoback, M. D. (2002, October). Deformation analysis in reservoir space (DARS): a simple formalism for prediction of reservoir deformation with depletion. In SPE/ISRM Rock Mechanics Conference. OnePetro.

[6] Zivar, D., Foroozesh, J., Pourafshary, P., & Salmanpour, S. (2019). Stress dependency of permeability, porosity and flow channels in anhydrite and carbonate rocks. Journal of Natural Gas Science and Engineering, 70, 102949.

[7] Rutqvist, J., Cappa, F., Rinaldi, A. P., & Godano, M. (2014). Modeling of induced seismicity and ground vibrations associated with geologic CO2 storage, and assessing their effects on surface structures and human perception. International Journal of Greenhouse Gas Control, 24, 64-77.

[8] Michael, K., Avijegon, A., Ricard, L., Strand, J., Freifeld, B., Woitt, M., ... & Geeves, D. (2018). The South West Hub In-Situ Laboratory–a facility for CO2 injection testing and monitoring in a fault zone.

[9] Song, J., & Zhang, D. (2013). Comprehensive review of caprock-sealing mechanisms for geologic carbon sequestration. Environmental science & technology, 47(1), 9-22.

[10] Streit, J. E., & Hillis, R. R. (2004). Estimating fault stability and sustainable fluid pressures for underground storage of CO2 in porous rock. Energy, 29(9-10), 1445-1456.

[11] Bond, C. E., Wightman, R., & Ringrose, P. S. (2013). The influence of fracture anisotropy on CO2 flow. Geophysical Research Letters, 40(7), 1284-1289.

[12] Heffer, K. J., Koutsabeloulis, N. C., & Wong, S. K. (1994, August). Coupled geomechanical, thermal and fluid flow modelling as an aid to improving waterflood sweep efficiency. In Rock mechanics in petroleum engineering. OnePetro.

[13] Fredrich, J. T., Arguello, J. G., Thorne, B. J., Wawersik, W. R., Deitrick, G. L., De Rouffignac, E. P., ... & Bruno, M. S. (1996, October). Three-dimensional geomechanical simulation of reservoir compaction and implications for well failures in the Belridge Diatomite. In SPE annual technical conference and exhibition. OnePetro.

[14] Fredrick, J. T., Deitrick, G. L., Arguello, J. G., & DeRouffignac, E. P. (1998, July). Reservoir compaction, surface subsidence, and casing damage: a geomechanics approach to mitigation and reservoir management. In SPE/ISRM rock mechanics in petroleum engineering. OnePetro.

[14] Settari, A., Sullivan, R.B., Walters, D.A., Wawrzynek, P. A., 2002. 3D analysis and prediction of microseismicity in fracturing by coupled geomechanical modeling. In SPE gas technology symposium. OnePetro.

[15] Sayers, C. M., Den Boer, L., Lee, D. W., Hooyman, P. J., & Lawrence, R. P. (2006, August). Predicting reservoir compaction and casing deformation in deepwater turbidites using a 3D mechanical earth model. In International oil conference and exhibition in Mexico. OnePetro.

[16] Qiu, K., Yamamoto, K., Birchwood, R. A., Chen, Y. R., Wu, C., Tan, C. P., & Singh, V. (2012, April). Evaluation of fault re-activation potential during offshore methane hydrate production in Nankai Trough, Japan. In Offshore technology conference. OnePetro..

[17] Qiu, K., Yamamoto, K., Birchwood, R., & Chen, Y. (2015). Well-integrity evaluation for methane-hydrate production in the deepwater Nankai Trough. SPE drilling & completion, 30(01), 52-67.

[18] Correa, A. C. F., Newman, R. B., Naveira, V. P., de Souza, A. L. S., Araujo, T., da Silva, A. A. C., ... & Meurer, G. B. (2013, October). Integrated modeling for 3D geomechanics and coupled simulation of fractured carbonate reservoir. In Otc Brasil. OnePetro.

[19] Yang, X., Pan, Y., Fan, W., Huang, Y., Zhang, Y., Wang, L., ... & Shan, F. (2018). Case study: 4D coupled reservoir/geomechanics simulation of a high-pressure/high-temperature naturally fractured reservoir. SPE Journal, 23(05), 1518-1538.

[20] Ahmed, B. I., & Al-Jawad, M. S. (2020). Geomechanical modelling and two-way coupling simulation for carbonate gas reservoir. Journal of Petroleum Exploration and Production Technology, 10(8), 3619-3648.

[21] Kim, J. (2010). Sequential methods for coupled geomechanics and multiphase flow. Stanford University.

[22] Mikelić, A., Wang, B., & Wheeler, M. F. (2014). Numerical convergence study of iterative coupling for coupled flow and geomechanics. Computational Geosciences, 18(3), 325-341.

[23] Alavi, M. (2004). Regional stratigraphy of the

Zagros fold-thrust belt of Iran and its proforeland evolution. American journal of Science, 304(1), 1-20.

[24] FALCON, N. L. (1961). Major earth-flexuring in the Zagros Mountains of south-west Iran. Quarterly Journal of the Geological Society, 117(1-4), 367-376.

[25] Motiei, H. (1993). Geology of Iran; Zagros Stratigraphy. Geological Society of Iran Publications.

[26] Darvishzadeh, A. (2009). Geology of Iran: stratigraphy, tectonic, metamorphism, and magmatism. Amir kabir, Tehran.

[27] James, G. A., & Wynd, J. G. (1965). Stratigraphic nomenclature of Iranian oil consortium agreement area. AAPG bulletin, 49(12), 2182-2245.

[28] Naim, A. E. M., & Alsharhan, A. S. (1997). Sedimentary basins and petroleum geology of the Middle East. Elsevier.

[29] Fjaer, E., Holt, R. M., Horsrud, P., & Raaen, A. M. (2008). Petroleum related rock mechanics. Elsevier.

[30] Zoback, M. D. (2007). Reservoir Geomechanics/Cambridge, New York, Melbourne: Cambridge University Press.

[31] Lacy, L. L. (1997, October). Dynamic rock mechanics testing for optimized fracture designs. In SPE annual technical conference and exhibition. OnePetro.

[32] Ameen, M. S., Smart, B. G., Somerville, J. M., Hammilton, S., & Naji, N. A. (2009). Predicting rock mechanical properties of carbonates from wireline logs (A case study: Arab-D reservoir, Ghawar field, Saudi Arabia). Marine and Petroleum Geology, 26(4), 430-444.

[33] Asef, M. R., & Farrokhrouz, M. (2010). Governing parameters for approximation of carbonates UCS. Electron J Geotech Eng, 15(2010), 1581-1592.

[34] Seyedsajadi, S., & Aghighi, M. A. (2015). Construction and Analysis of a Geomechanical Model for Bangestan Reservoir in Koopal Field. Iranian Journal of Mining Engineering, 10(26), 21-34.

[35] Jaeger, J. C., Cook, N. G., & Zimmerman, R. (2009). Fundamentals of rock mechanics. John Wiley & Sons.

[36] Plumb, R. A. (1994). Influence of composition and texture on the failure properties of clastic rocks. Rock Mechanics in Petroleum Engineering. Society of Petroleu m Engineers.

[37] Eaton, B. A. (1975, September). The equation for geopressure prediction from well logs. In Fall meeting of the Society of Petroleum Engineers of AIME. OnePetro.

[38] Torsvik, T. H., Van der Voo, R., Preeden, U., Mac Niocaill, C., Steinberger, B., Doubrovine, P. V., ... & Cocks, L. R. M. (2012). Phanerozoic polar wander, palaeogeography and dynamics. Earth-Science Reviews, 114(3-4), 325-368.

[39] Azadpour, M., & Shad Manaman, N. (2015). Determination of pore pressure from sonic log: a case study on one of Iran carbonate reservoir rocks. Iranian Journal of Oil and Gas Science and Technology, 4(3), 37-50.

[40] Kidambi, T., & Kumar, G. S. (2016). Mechanical earth modeling for a vertical well drilled in a naturally fractured tight carbonate gas reservoir in the Persian Gulf. Journal of Petroleum Science and Engineering, 141, 38-51.

[41] Tabaeh, H. M., & Mohammad, A. (2016). Estimation of in-situ horizontal stresses using the linear poroelastic model and minifrac test results in tectonically active area. Russian Journal of Earth Sciences, 16(4), 1-9.

[42] Krief, M., Garat, J., Stellingwerff, J., & Ventre, J. (1990). A petrophysical interpretation using the velocities of P and S waves (full-waveform sonic). The Log Analyst, 31(06).

[43] Rutqvist, J., Birkholzer, J., Cappa, F., & Tsang, C. F. (2007). Estimating maximum sustainable injection pressure during geological sequestration of CO2 using coupled fluid flow and geomechanical fault-slip analysis. Energy Conversion and Management, 48(6), 1798-1807.

[44] Tillner, E., Shi, J. Q., Bacci, G., Nielsen, C. M., Frykman, P., Dalhoff, F., & Kempka, T. (2014). Coupled dynamic flow and geomechanical simulations for an integrated assessment of CO2 storage impacts in a saline aquifer. Energy Procedia, 63, 2879-2893.

[45] Tran, D., Nghiem, L., & Buchanan, L. (2005, November). An overview of iterative coupling between geomechanical deformation and reservoir flow. In SPE international thermal operations and heavy oil symposium. OnePetro.

[46] Wang, C., Wu, Y. S., Xiong, Y., Winterfeld, P. H., & Huang, Z. (2015, February). Geomechanics coupling simulation of fracture closure and its influence on gas production in shale gas reservoirs. In SPE reservoir simulation symposium. OnePetro.

[47] Kim, S., & Hosseini, S. A. (2014). Geological CO2 storage: Incorporation of pore-pressure/stress coupling and thermal effects to determine maximum sustainable pressure limit. Energy Procedia, 63, 3339-3346.

[48] van Thienen-Visser, K., Pruiksma, J. P., & Breunese, J. N. (2015). Compaction and subsidence of the Groningen gas field in the Netherlands. Proceedings of the International Association of Hydrological Sciences, 372, 367-373.